

Supporting Information

Multi-strategy preparation of efficient and stable environment-friendly lead-based perovskite solar cells

Huan Bi,^{a,b} Gaoyi Han,^b Mengna Guo,^b Chao Ding,^a Hanjun Zou,^c Qing Shen,^{a*} Shuzi Hayase^{a*} and Wenjing Hou^{b*}

^a Graduate School of Informatics and Engineering, The University of Electro-Communication, Tokyo 182-8585, Japan.

^b Institute of Molecular Science, Key Laboratory of Materials for Energy Conversion and Storage of Shanxi Province, Shanxi University, Taiyuan 030006, P. R. China

^c Analytical and Testing Center, Chongqing University, Chongqing 401331, China

*** Corresponding Author**

E-mail: shen@pc.uec.ac.jp

E-mail: hayase@uec.ac.jp

E-mail: houwenjing@sxu.edu.cn

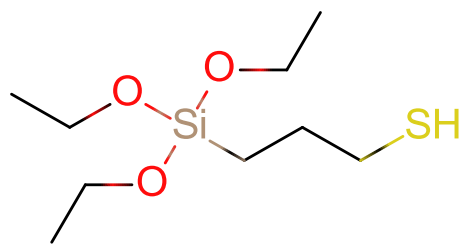


Figure S1. The structure of the SiSH.

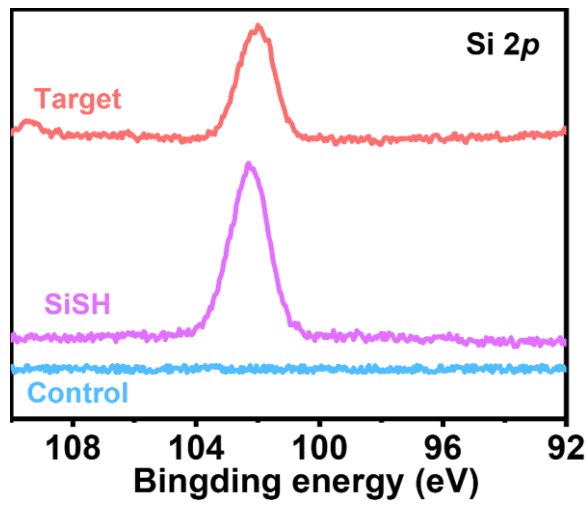


Figure S2 Si 2p XPS spectra of bare perovskite film, SiSH, and the perovskite film prepared by SiSH dissolved in CB

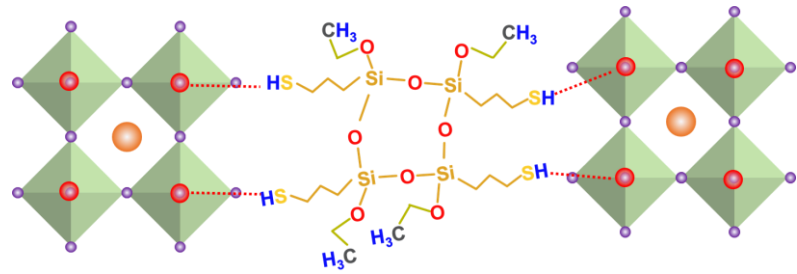


Figure S3. Proposed mechanism of crystallization modulation and defect passivation achieved by the functionalized cross-linking agent.

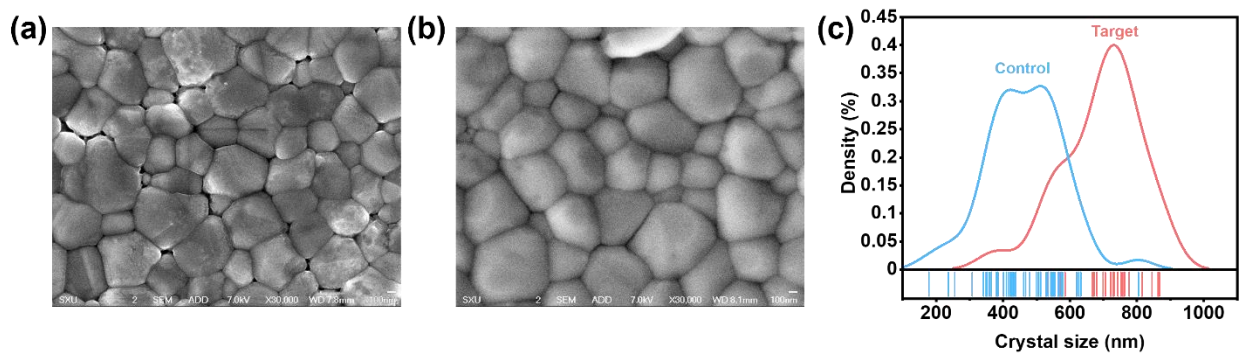


Figure S4. SEM images of the perovskite thin film **a** without or **b** with SiSH treated. **c** the corresponding grain sizes statistics.

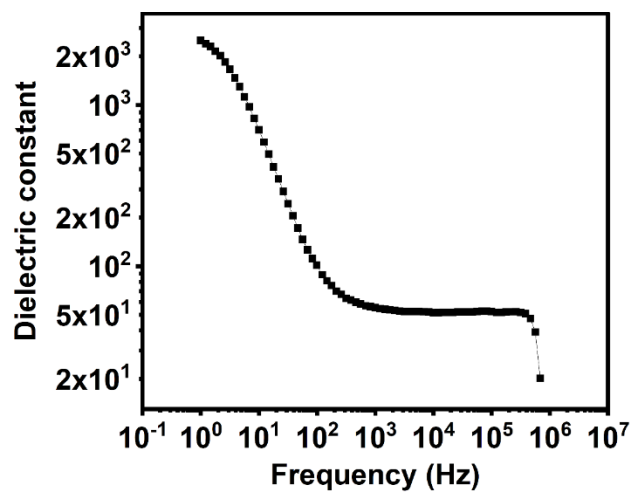


Figure S5. C-f curve with the structure of ITO/perovskite/Au. Here, the dielectric constant was used with the frequency of 10K Hz^1 .

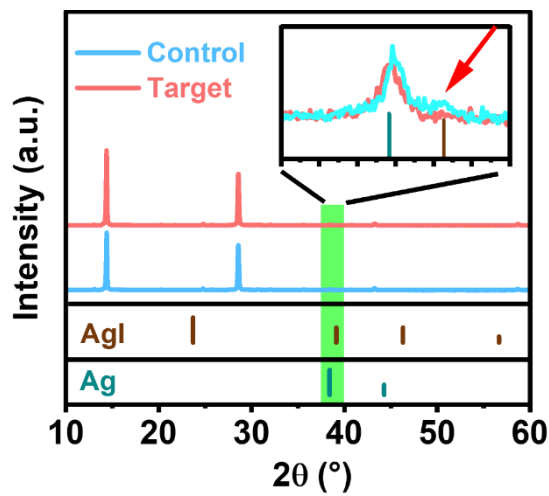


Figure S6. XRD measurement of the perovskite thin-film covered with Ag.

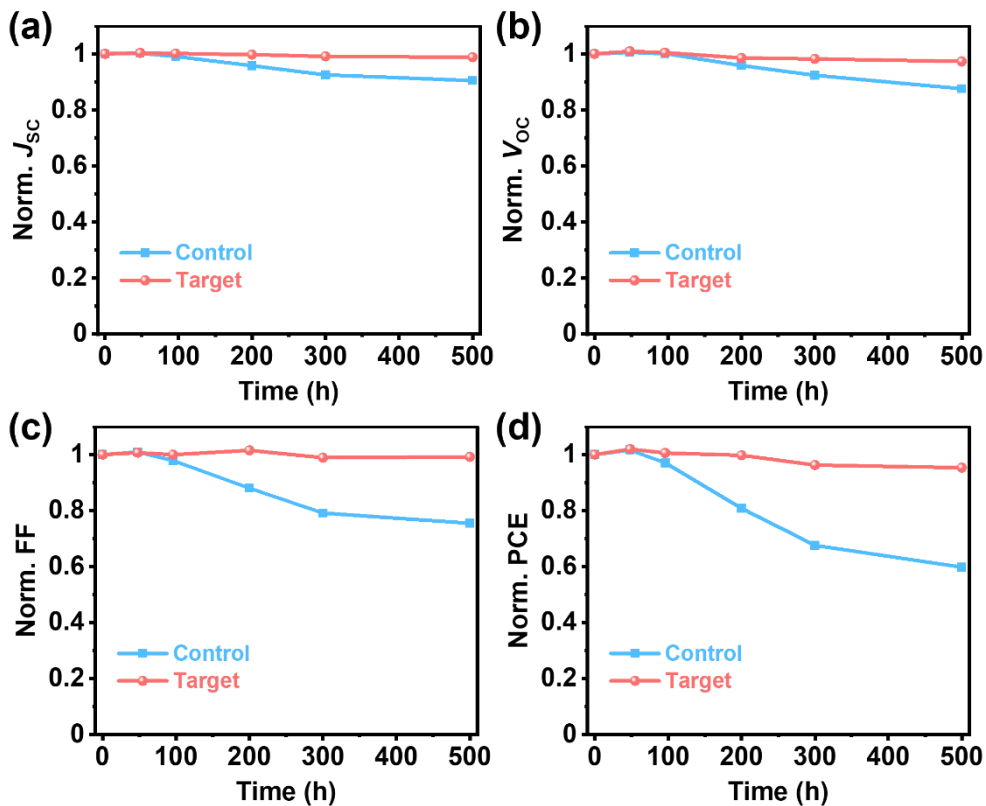


Figure S7. **a** Normalized J_{SC} , **b** Normalized V_{OC} , **c** Normalized FF, and **d** Normalized PCE as a function of time for the unencapsulated devices exposed to the humidity of 40-45 RH% at room temperature in the dark.

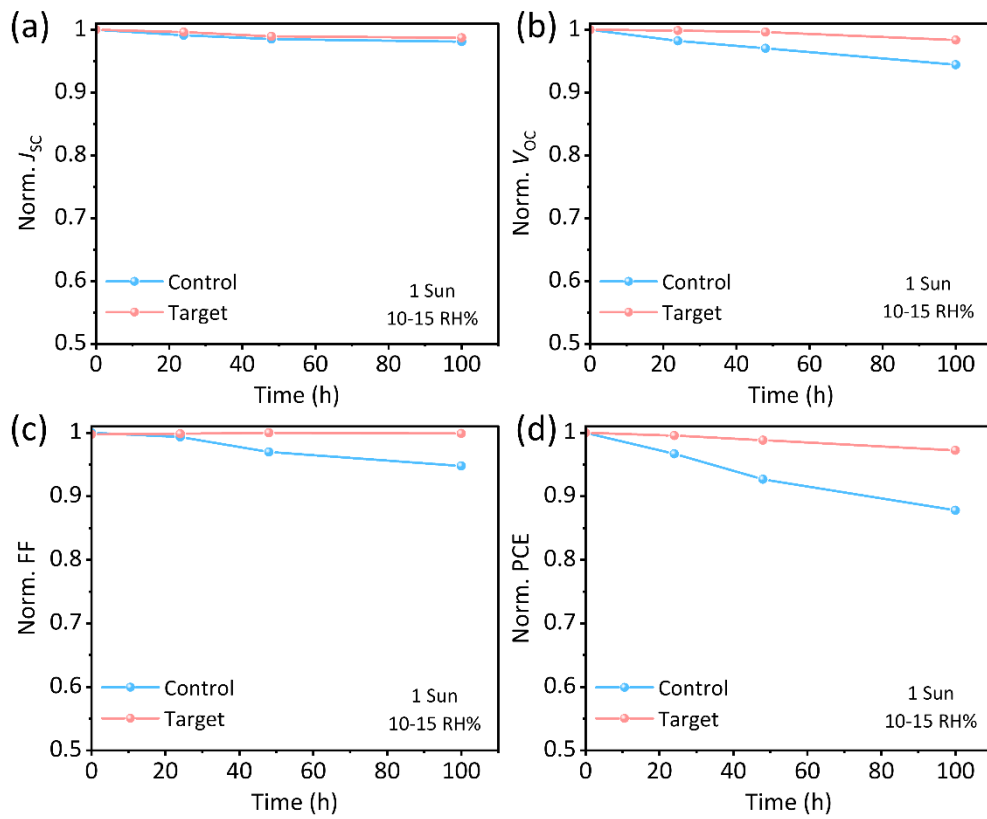


Figure S8. **a** Normalized J_{SC} , **b** Normalized V_{OC} , **c** Normalized FF, and **d** Normalized PCE as a function of time for the unencapsulated devices under one sun illumination and in the air condition with the humidity of 10-15 RH% at room temperature.

Table S1. Photovoltaic parameters of the PSCs with different concentrations of SiSH dissolved in CB from 0 to 12 μ L/mL

SiSH (μ L/mL)		J_{SC} (mA/cm ²)	V_{OC} (V)	FF	PCE (%)
	Champion	24.72	1.09	0.772	20.80
0	Average	24.70	1.09	0.771	20.67
	Std. Dev.	0.124	0.004	0.001	0.074
	Champion	24.91	1.11	0.786	21.64
4	Average	24.76	1.11	0.785	21.56
	Std. Dev.	0.110	0.003	0.003	0.063
	Champion	24.99	1.12	0.801	22.42
8	Average	24.83	1.12	0.798	22.21
	Std. Dev.	0.135	0.002	0.002	0.127
	Champion	24.84	1.11	0.791	21.87
12	Average	24.79	1.11	0.791	21.71
	Std. Dev.	0.120	0.004	0.003	0.082

Table S2. Summarized the additive strategies to obtain high PCE and environment-friendly device.

Device structure	J _{SC} (mA/cm ²)	V _{OC} (V)	FF	PCE (%)	Ref.
FTO/TiO ₂ /PVK/CuP/Spiro/Au	23.91	1.14	79.32	21.76	²
ITO/PTAA/PVK/C60/SnO ₂ /Carbon	21.90	0.87	56.30	10.70	³
FTO/TiO ₂ /PVK/Spiro/Au	23.39	1.14	76.00	20.27	⁴
FTO/SnO ₂ /PVK/Spiro/Au	23.20	1.14	79.80	21.20	⁵
ITO/PTAA/PVK/PC61BM/EEL/Ag	22.58	1.20	81.28	22.02	⁶
FTO/TiO ₂ -SnO ₂ /S-PVK/Spiro /Ag	22.80	1.08	79.00	19.45	⁷
ITO/PTAA/PVK/C60/BCP/Cu	22.50	1.13	80.60	20.6	⁸
FTO/TiO ₂ / PVK /Spiro/Au	23.43	1.14	79.50	21.22	⁹
ITO/NiOx/PVK/PCBM+C60/BCP/Cr/Au	23.53	1.13	83.10	22.07	¹⁰
FTO/TiO ₂ / PVK /Spiro/Au	24.45	1.17	81.21	23.23	¹¹
ITO/PTAA/PVK/C60/ BCP/Ag	22.47	1.14	81.00	21.00	¹²
ITO/SnO ₂ /PVK/PTAA/Ag	25.55	1.15	79.88	23.55	¹³
ITO/SnO ₂ /PVSK/Spiro/Ag	24.99	1.12	80.10	22.42	This work

Table S3. Fitting results from TRPL dynamics in Figure 2e.

	Glass/PVK	Glass/ PVK (SiSH in CB)
τ_1 (ns)	14.15	33.84
%	86.56	62.77
τ_2 (ns)	144.27	169.44
%	13.44	37.23
τ_{ave} (ns)	69.85	135.28

Supplementary Note 1

TAS analysis is an effective method for understanding the energy profile of trap-states in PSCs. These methods can generally reach a trap depth of ~0.55 eV from the conduction band or VB edge, which is normally deep enough for most low-bandgap PSCs. Previous reports revealed that the trap states in energy space can be divided into three regions, among which the deep trap depth regions (zones II and III) are mainly related to the surface defects and the shallower trap-states (zone I) are more closely related to the bulk or grain boundaries of perovskite.¹⁴

The TAS measurements were carried out with the DC bias at 0 V and AC bias at 0.02 V. The scanning range of the AC frequency ranged from 100 Hz to 1 MHz. The energy profile of trap density of states (*t*DOSs) can be derived from the angular frequency-dependent capacitance by using the following equation:¹⁵

$$N_t(E_\omega) = -\frac{V_{bi}}{qW} \frac{dC}{d\omega} \frac{\omega}{k_B T}$$

where ω is the angular frequency, k_B is the Boltzmann's constant, and T is the temperature. W represents depletion width, approximately equal to the thickness of perovskite thickness (in general, the material is assumed to be completely depleted). V_{bi} is the built-in potential, which was extracted from the Mott–Schottky analysis. The energetic demarcation (E_ω) is defined by using angular frequency $E_\omega = k_B T \ln(\frac{\omega_0}{\omega})$, where ω_0 is the attempt to escape frequency that was estimated to be $\sim 1.0 \times 10^{12}$ Hz for $\text{FA}_{0.91}\text{Cs}_{0.07}\text{MA}_{0.05}\text{PbI}_{2.88}\text{Br}_{0.15}$ perovskite active layer.¹⁶

Video S1. Video of control film soaked in water. (MP4);
Video S2. Video of target film soaked in water. (MP4);
Video S3. Video of control film soaked in acid rain. (MP4);
Video S4. Video of target film soaked in acid rain. (MP4);
Video S5. Video of Pb recovery

References

1. Liu, Y.; Xu, Z.; Yang, Z.; Zhang, Y.; Cui, J.; He, Y.; Ye, H.; Zhao, K.; Sun, H.; Lu, R.; Liu, M.; Kanatzidis, M. G.; Liu, S. Inch-size 0D-structured Lead-Free Perovskite Single Crystals for Highly Sensitive Stable X-Ray Imaging. *Matter* **2020**, *3*, 180-196.
2. Xiao, G.-B.; Wang, L.-Y.; Mu, X.-J.; Zou, X.-X.; Wu, Y.-Y.; Cao, J. Lead and Iodide Fixation by Thiol Copper(II) Porphyrin for Stable and Environmental-Friendly Perovskite Solar Cells. *CCS Chemistry* **2021**, *3*, 25-36.
3. Chen, S.; Deng, Y.; Gu, H.; Xu, S.; Wang, S.; Yu, Z.; Blum, V.; Huang, J. Trapping Lead in Perovskite Solar Modules with Abundant and Low-Cost Cation-Exchange Resins. *Nat. Energy* **2020**, *5*, 1003-1011.
4. Li, X.; Zhang, F.; He, H.; Berry, J. J.; Zhu, K.; Xu, T. On-device Lead Sequestration for Perovskite Solar Cells. *Nature* **2020**, *578*, 555-558.
5. Lee, J.; Kim, G.-W.; Kim, M.; Park, S. A.; Park, T. Nonaromatic Green-Solvent-Processable, Dopant-Free, and Lead-Capturable Hole Transport Polymers in Perovskite Solar Cells with High Efficiency. *Adv. Energy Mater.* **2020**, *10*, 1902662.
6. Wu, S.; Li, Z.; Li, M.-Q.; Diao, Y.; Lin, F.; Liu, T.; Zhang, J.; Tieu, P.; Gao, W.; Qi, F.; Pan, X.; Xu, Z.; Zhu, Z.; Jen, A. K. Y. 2D Metal–organic Framework for Stable Perovskite Solar Cells with Minimized Lead Leakage. *Nat. Nanotechnol.* **2020**, *15*, 934-940.
7. Xie, L.; Zhang, T.; Zhao, Y. Stabilizing the MAPbI₃ Perovksite via the In-situ Formed Lead Sulfide Layer for Efficient and Robust Solar Cells. *J. Energy Chem.* **2020**, *47*, 62-65.
8. Chen, S.; Deng, Y.; Xiao, X.; Xu, S.; Rudd, P. N.; Huang, J. Preventing Lead Leakage with Built-in Resin Layers for Sustainable Perovskite Solar Cells. *Nat. Sustain.* **2021**, *4*, 636-643.
9. Li, X.; Zhang, F.; Wang, J.; Tong, J.; Xu, T.; Zhu, K. On-device Lead-absorbing Tapes for Sustainable Perovskite Solar Cells. *Nat. Sustain.* **2021**, *4*, 1038-1041.
10. Cao, Q.; Wang, T.; Yang, J.; Zhang, Y.; Li, Y.; Pu, X.; Zhao, J.; Chen, H.; Li, X.; Tojiboyev, I.; Chen, J.; Etgar, L.; Salari, H.; Li, X. Environmental-Friendly Polymer for Efficient and Stable Inverted Perovskite Solar Cells with Mitigating Lead Leakage. *Adv. Funct. Mater.* **2022**, *n/a*, 2201036.
11. Hu, Y.; Song, W.; Wang, X.; Shi, X.; Jia, X.; He, Z.; Zhang, S.; Yuan, G.; Wang, M.; Wang, J.; Sun, G.; Sun, T.; Tang, Y. A Holistic Sunscreen Interface Strategy to Effectively Improve the

Performance of Perovskite Solar Cells and Prevent Lead Leakage. *Chem. Eng. J.* **2022**, *433*, 134566.

12. Li, Z.; Wu, X.; Wu, S.; Gao, D.; Dong, H.; Huang, F.; Hu, X.; Jen, A. K. Y.; Zhu, Z. An Effective and Economical Encapsulation Method for Trapping Lead Leakage in Rigid and Flexible Perovskite Photovoltaics. *Nano Energy* **2022**, *93*, 106853.
13. Wei, X.; Xiao, M.; Wang, B.; Wang, C.; Li, Y.; Dou, J.; Cui, Z.; Dou, J.; Wang, H.; Ma, S.; Zhu, C.; Yuan, G.; Yang, N.; Song, T.; Zhou, H.; Chen, H.; Bai, Y.; Chen, Q. Avoiding Structural Collapse to Reduce Lead Leakage in Perovskite Photovoltaics. *Angew. Chem. Int. Ed.* **2022**, *n/a*, e202204314.
14. Ni, Z.; Bao, C.; Liu, Y.; Jiang, Q.; Wu, W.-Q.; Chen, S.; Dai, X.; Chen, B.; Hartweg, B.; Yu, Z.; Holman, Z.; Huang, J. Resolving spatial and energetic distributions of trap states in metal halide perovskite solar cells. *Science* **2020**, *367*, 1352-1358.
15. Shao, Y.; Xiao, Z.; Bi, C.; Yuan, Y.; Huang, J. Origin and elimination of photocurrent hysteresis by fullerene passivation in $\text{CH}_3\text{NH}_3\text{PbI}_3$ planar heterojunction solar cells. *Nat. Commun.* **2014**, *5*, 5784.
16. Zhang, F.; Ye, S.; Zhang, H.; Zhou, F.; Hao, Y.; Cai, H.; Song, J.; Qu, J. Comprehensive passivation strategy for achieving inverted perovskite solar cells with efficiency exceeding 23% by trap passivation and ion constraint. *Nano Energy* **2021**, *89*, 106370.